Materials Science-Poland
Volume 43 Issue 3 · pp. 202–215 · DOI: 10.2478/msp-2025-0038

Materials Science-Poland

Fluorescent yttrium oxide nanoparticles for sensitive detection of vitamin B_{12}: Synthesis, characterization, and sensor development

Research Article

Salma Alshehri[1], Mohammad Shariq[2]*, Wafa Al-Gethami[3], Aisha H. Al-Moubaraki[4], M. D. Alshahrani[1], Nouf Alharbi[2], Hind S. Alzahrani[5], Noha Al-Qasmi[3]

[1] *Department of Physics, College of Science, University of Bisha, P. O. Box 551, Bisha 61922, Saudi Arabia*
[2] *Department of Physical Sciences, Physics Division, College of Science, Jazan University, P.O. Box 114, Jazan 45142, Saudi Arabia*
[3] *Department of Chemistry, College of Science, Taif University, Taif 21944, Saudi Arabia*
[4] *Department of Chemistry, College of Science, University of Jeddah, Jeddah 21589, Saudi Arabia*
[5] *Department of Physics, College of Science, Taif University, P. O. Box 11099, Taif 21944, Saudi Arabia*

Received 15 August 2025; Accepted 04 November 2025

Abstract: A fluorescent yttrium oxide nanoparticle was successfully synthesized and employed as a fluorometric probe for the detection of vitamin B_{12}. The sensing mechanism is based on the interaction between vitamin B_{12} and the nanoparticles, enabling sensitive fluorescence measurements. The material was thoroughly characterized using X-ray diffraction, scanning electron microscopy, energy dispersive X-ray spectroscopy, photoluminescence, high-resolution transmission electron microscopy, Fourier-transform infrared spectroscopy, X-ray photoelectron spectroscopy, and UV-Visible spectroscopy. The strongest fluorescence response was obtained at an excitation wavelength of 230 nm and an emission wavelength of 285 nm. Key parameters, including pH, incubation time, and NaCl concentration, were systematically optimized. The probe demonstrated a linear response in the vitamin B_{12} concentration range of 10–100 µM, with a limit of quantification of 55.66 µM and a detection limit of 18.37 µM. Additionally, an red, green, blue color based sensor was developed using the same nanoparticles, which successfully detected vitamin B_{12} with high accuracy in human urine samples and acceptable recovery, highlighting its potential for real-world biomedical applications.

Keywords: *Fluorescence • Nanoparticles • Sensors • Smartphone • Vitamin B_{12}*

1. Introduction

Vitamin B_{12} is a cobalt-containing chemical complex that is required for human health. Vitamin B_{12}, present in the active coenzyme forms methylcobalamin and adenosylcobalamin, plays a vital role in cellular development, growth, and metabolic regulation, while cyanocobalamin serves as a synthetic precursor commonly used in supplementation. Deficiency in this vitamin can result in pernicious anemia, weakness, nausea, and fatigue [1,2]. Vitamin B_{12} is an essential coenzyme that plays a crucial role in cellular growth and development. As the human body is unable to produce this vitamin, it needs to be supplemented through food items like dairy products, fish, eggs, meat, oysters, and poultry. Plant foods have very minimal amounts of vitamin B_{12}, so vegetarians and those who do not consume red meat need supplementation [3,4]. Vitamin B_{12} is crucial for producing red blood cells, DNA synthesis, neurological function, and a healthy immune system. Deficiency may cause low energy levels, muscle weakness, and gastrointestinal disturbances, as well as neurological features of peripheral neuropathy and dementia. Biochemically, it leads to the rise in homocysteine and methylmalonic acid, which in turn add to systemic and neurological complications, thus having a profound impact on life expectancy [5,6]. Vitamin B_{12}, produced only by microorganisms, is obtained mainly from animal-derived foods, while plant foods lack it unless fortified. Vitamin B_{12} is used as a cofactor by L-methylmalonyl-CoA mutase and methionine synthase, the latter of which converts

* *E-mail: aligshariq@gmail.com, mohammadshariq@jazanu.edu.sa*

homocysteine into the amino acid methionine. Deficiency is usually identified by a complete blood count and a vitamin B_{12} blood test.

For the detection of vitamin $B_{12,}$ several analytical techniques have been described, such as high-performance liquid chromatography, electrochemical detection, enzyme-linked immunosorbent assay, and microbiological tests [7–9]. Though satisfactory, these methods are hampered by being costly and complex in instrument requirements, labor, and trained personnel. Furthermore, the absence of a standardized procedure complicates routine analysis. New developments have proposed new alternatives; for instance, the use of a time-resolved fluorescent microsphere immunochromatographic assay allowed rapid and ultrasensitive detection of vitamin B_{12} in infant formula with high accuracy and stability [10]. In the same line, yellow-emissive carbon dots prepared through a one-pot hydrothermal process were employed as a label-free fluorescent probe with a low detection limit of 0.1 μM and successful application to real samples [11]. Other methods are the application of magnetic nanoparticles to selectively enrich and preconcentrate cyanocobalamin, which enhances sensitivity in matrices that are complex [12]. Optical methods commonly depend on noble metals (such as gold, silver, and platinum) or heavy-metal-doped quantum dots, posing cost and toxicity issues, yet fluorescence-based sensing with non-metal-doped quantum dots has attracted much interest due to its high sensitivity, low cost, simplicity in operation, and possibility of direct visual detection.

Nanoparticles are hybrid or heterogeneous materials designed at the nanometric level, possessing different properties from their bulk form. Their structures are more complex than those of micro-composites [13]. Because of their heterogeneity, the properties of nanoparticles are dependent on factors related to those in conventional composites, such as component properties, composition, structure, and interfacial interactions [14]. The nanoscale nature of these particles changes their atomic characteristics, resulting in improved functionalities. This change in nanoparticle characteristics has been beneficial in different applications (biomedical applications/sensors, optical filters, solar cells, etc.) [15–18].

Yttrium oxide (YTO) is a highly promising material for developing advanced architectures with applications in photocatalysis [19], sensing [20], biosensing [21], and hydrogen production [22]. Its widespread interest stems from its biocompatibility and non-toxicity, making it suitable for eco-friendly systems and biomedical applications [23,24]. The most common crystalline form of YTO is hexagonal, serving as the foundation for various morphologies, including hexagonal plates, cones (needles), and prisms (rods or tubes) [25]. These morphologies can be tailored by controlling preferential growth directions. Additionally, hydrothermal synthesis provides a straightforward method for fabricating diverse YTO nanostructures, with temperature and solution alkalinity playing crucial roles in influencing nanoparticle growth. It is an extensively used transition metal oxide and has high potential for future development because of its superior mechanical [26], chemical [27], and thermal stability [28]. It is an established host matrix for luminescent ions and has recently come into focus as an integral part of transition materials. YTO is an excellent raw material for chemical catalysis and optoelectronic devices, besides other applications in biological systems and photodynamic imaging. Additionally, it is commonly used as a dopant for rare-earth doping. Through the reduction in electron-hole pair combination, the creation of innovative active sites, and the enhancement of material properties through synergistic effects, YTO might be combined with additional non-metals, metals, lanthanides, and oxides to improve photocatalytic, optoelectronic, and antibacterial capabilities [17].

Literature on the application of YTO nanoparticles for the optical sensing of vitamin B_{12} has not been reported, as per our literature review. But some limited research has been done with similar oxide nanomaterials, like iron oxide, zinc oxide, and rare-earth-doped oxides, for sensing vitamins, in which they have shown highly positive optical and catalytic features. But as yet, no report is available specifically for YTO, demonstrating a definite lacuna in this regard. This gap, together with the need for in-depth research on the role of metal oxides in composite properties with sensing implications, motivated this study. The goal of this research was to synthesize and characterize YTO nanoparticles and examine how their concentration affects structural, vibrational, morphological, optical, and surface features. To achieve this, we used a set of sophisticated characterization tools: X-ray diffraction (XRD) to identify crystal structure and phase purity; transmission electron microscopy (TEM) and scanning electron microscopy (SEM) to investigate particle size, shape, and morphology; Fourier-transform infrared spectroscopy (FT-IR) to determine functional groups and surface interactions; X-ray photoelectron spectroscopy (XPS) to investigate surface composition and oxidation states; UV-Visible (UV-Vis) spectroscopy to investigate optical absorption; and photoluminescence (PL) spectroscopy to investigate emission properties for assessment of sensing performance. Consequently, the novelty of our work lies in the

development and thorough characterization of a nanomaterial with potential applications in optical sensing.

2. Materials and procedures

2.1 Materials

Deionized water from the Millipore Milli-Q water purification system was used to create the solution, having a resistivity of 18.2 MΩ cm. Analytical-grade hydrochloric acid and sodium hydroxide, used in pH maintenance studies, were bought from Loba, India. Vitamin B_{12} and melatonin were acquired from Sigma Aldrich. A few other substances, including sodium chloride, glycine, lysine, biotin, riboflavin, dopa, yttrium nitrate, phenylalanine, ammonia, and tryptophan, were acquired from Loba. Distilled water was employed as the reference solution in the measurements.

2.2 YTO synthesis

0.725 g of yttrium nitrate was dissolved in 20 mL of distilled water using a magnetic stirrer and stirred constantly at 6,000 rpm for 2 h. When a clear solution was obtained, it was placed in a crucible and calcined at 500°C for 1 h, giving a white solid. The product was filtered and washed with ethanol and distilled water in 1:1 ratio, and then dried at 60°C, as shown in Figure 1.

2.3 Characterization techniques

The YTO nanoparticles were also characterized with FTIR, TEM, XRD, XPS, SEM, PL and UV-Vis spectroscopic methods. The size and surface particle morphology were determined by high-resolution TEM (HR-TEM, JEOL-2010 microscope running at 300 kV). Topography and thickness information were gathered with an Agilent 5500 SEM. The crystallinity of YTO was determined on an XRD (P-Analytical Empyrean), and chemical classes of metal oxides and their binding energies were detected with an XPS (Thermo Fisher Scientific EscaLab Xi+) of Physical Electronics. The UV-Vis absorption spectra were noted by a Lab-India UV-Vis spectrometer. The fluorescence spectra of YTOs were monitored by a fluorescence spectrophotometer (Hitachi FL-4600 spectrophotometer) in the range of 200–270 nm excitation wavelengths. Furthermore, surface functional groups on the material were detected through an FT-IR spectrophotometer (Agilent Cary 630).

2.4 Optical sensing of vitamin B_{12}

A fluorescence spectrophotometer (with λ_{ex} = 230 nm) was utilized to see the fluorescence spectra and intensities of YTO solution (10^{-3} M) after various quantities of vitamin B_{12} (10^{-4} M) were introduced into the solution, and distilled water was used as the solvent for all experiments in this study. The experiment was conducted three times for quality control. At room temperature, the vitamin B_{12} diagnostic procedure was performed. Various vitamins, amino acids, and metal ions were introduced to YTO solution under the same circumstances as vitamin B_{12} to further estimate the selectivity of the nano-sensing system for this nutrient.

2.5 Optimization conditions

In various challenging conditions, including UV lamp exposure, high-salinity solutions, pH fluctuations, and prolonged stress, the stability and exceptional properties of YTO were thoroughly examined to enhance its applicability. Notably, the fluorescence intensity of YTO remained consistent across a wide range of sodium chloride salt concentrations (1–5 M), demonstrating remarkable stability even in environments with high ionic strength (5 M, Figure 2a). This resilience suggests that YTO can effectively resist quenching from salts and other adverse factors, making it highly valuable for environmental and sensing applications. Furthermore, when subjected to UV lamp radiation, YTO

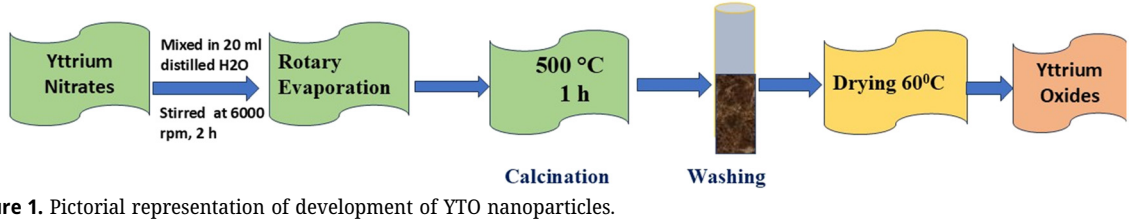

Figure 1. Pictorial representation of development of YTO nanoparticles.

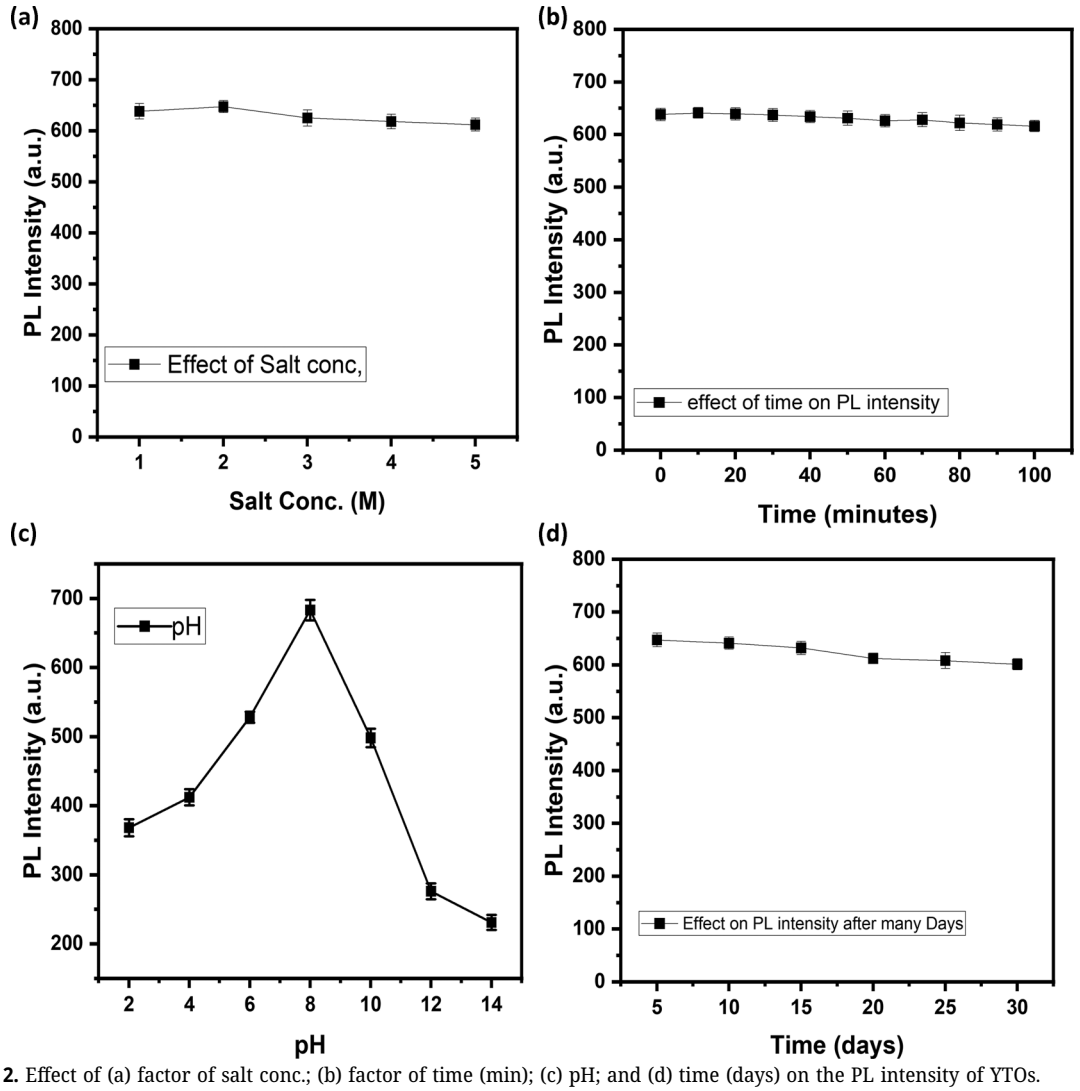

Figure 2. Effect of (a) factor of salt conc.; (b) factor of time (min); (c) pH; and (d) time (days) on the PL intensity of YTOs.

exhibited outstanding photostability, with its PL intensity showing negligible variation even after 100 min of continuous exposure (Figure 2b). This property highlights its superior resistance to photobleaching, further reinforcing its potential for long-term use in demanding conditions. For sensor applications, it is essential to maintain steady fluorescence intensity to ensure accurate and reproducible observations. YTO is an appropriate selection for monitoring the environment tasks necessitating reliable and accurate detection of analytes or pollutants, as its fluorescence intensity stays steady at high ionic strength circumstances. Furthermore, fluorescence stability across numerous pH solutions was evaluated, with the results presented in Figure 2c. In acidic conditions (pH 2–5), fluorescence intensity was initially low. However, it peaked between pH 7 and 8 before declining at higher pH levels. This reduction in fluorescence intensity at elevated pH values can be credited to factors such as surface passivation layer degradation, nanoparticle aggregation, and other chemical changes [29,30].

These findings highlight YTO's significant potential for use in various fields, including sensing and environmental studies. Notably, the fluorescence peaks of YTO remained stable over a 1-month period (Figure 2d), indicating excellent long-term stability. Continuous sensing and long-term environmental monitoring are two examples of applications that require fluorescence performance that is consistent over lengthy periods of time. This stability is therefore crucial for these applications [31,32]. Additionally, Figure 6c presents the emission spectra of YTO at

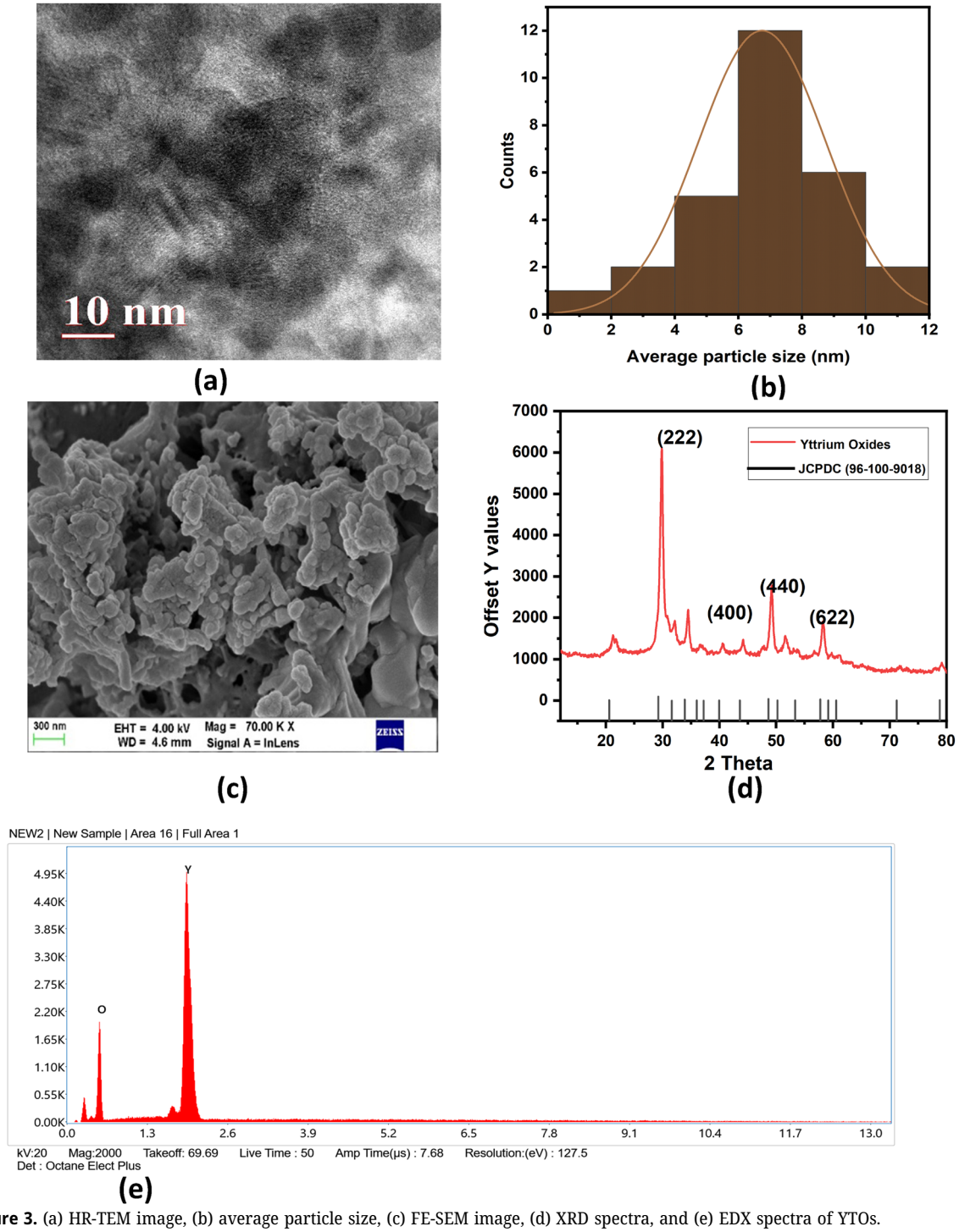

Figure 3. (a) HR-TEM image, (b) average particle size, (c) FE-SEM image, (d) XRD spectra, and (e) EDX spectra of YTOs.

different excitation wavelengths fluctuating from 200 to 270 nm. The PL intensity at 285 nm initially increases with excitation from 200 to 230 nm, followed by a decline in the 240–270 nm range. The results show that the emission wavelength of YTO, which peaks at 230 nm, is unaffected by the excitation wavelength.

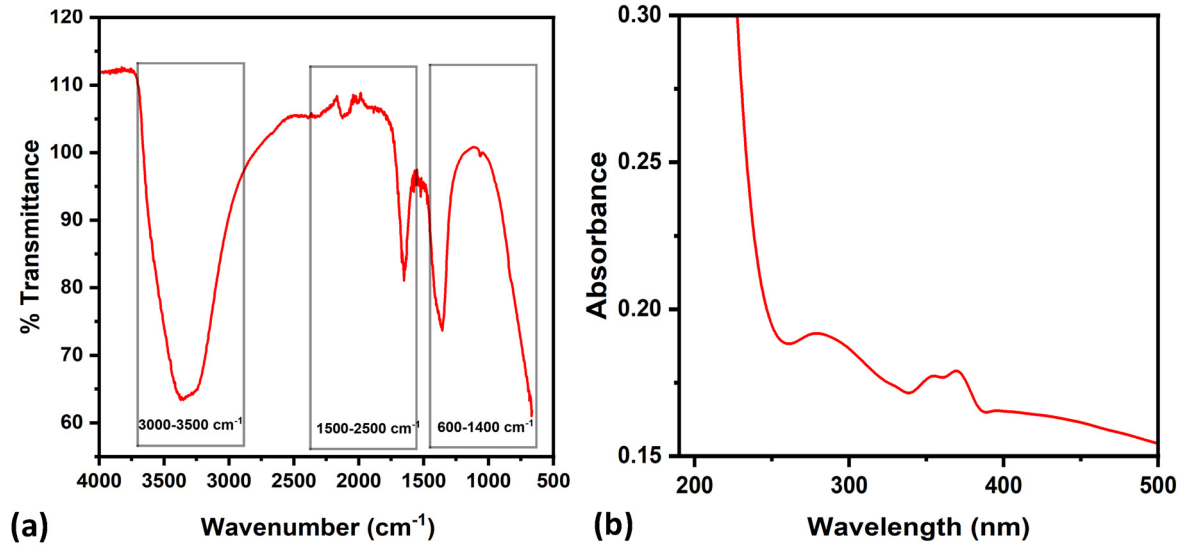

Figure 4. (a) FT-IR spectra and (b) UV-Vis absorption spectrum of YTO.

2.6 Detection of vitamin B_{12} using YTO

Fluorescence-based sensing experiments were performed to sense vitamin B_{12} with high sensitivity. Vitamin B_{12} concentration was shown to cause a linear dampening of YTO fluorescence intensity. The fluorescence quenching equation was used to compute the Stern–Volmer constant (K_{sv}) [33]:

$$I_0/I = 1 + [Q]K_{sv}, \quad (1)$$

where [Q] is the vitamin B_{12} concentration, and (I_0) and (I) are the YTOs fluorescence intensities at 285 nm without and with vitamin B_{12}, respectively [34].

3. Results and discussion

3.1 Analysis methods

TEM was used to study the structural and morphological characteristics of YTO nanoparticles. HR-TEM images showed clearly defined nanostructures with a fairly homogeneous size distribution and visible lattice fringes, attesting to the crystalline nature of the material (Figure 3a). The particles showed predominantly spherical or slightly irregular shapes, ranging in nanometer size [35]. The observation of lattice fringes in HR-TEM images also signified well-ordered atomic structures, implying high purity and phase stability. Apart from morphology, TEM analysis further indicated a propensity of some nanoparticles to self-assemble into small aggregates, a feature typically found in oxide nanoparticles because of high surface energy and van der Waals forces [36]. Such an aggregation can impact surface reactivity and optical properties, although in some cases, it can also lead to improved stability. The microstructural characteristics also indicate the existence of voids and interparticle voids, as consistent with mesoporous features commonly described for rare-earth oxides [37]. This porosity increases the surface area, thereby enhancing analyte interactions and improving performance in sensing and catalysis. Figure 3b illustrates the particle size distribution histogram of YTO nanoparticles, fitted with a log-normal distribution curve, exhibiting a mean particle size of 7.0 ± 1.8 nm and an R^2 value of 0.96, indicating a good fit.

SEM imaging (Figure 3c) validated the nanoscale nature of the particles, though particle size and shape variations were apparent, further corroborating the partial aggregation tendency. The EDX spectrum (Figure 3e) confirmed the elemental structure of the nanoparticles with robust signals for yttrium and oxygen, determining material purity. These findings collectively suggest that YTO nanoparticles have a crystalline, porous, and partially aggregated morphology, characteristics that make them more favorable as sensing, catalysis, and optoelectronic device materials.

XRD examination was conducted to ascertain phase formation and crystalline structure of YTO nanoparticles, as shown in Figure 3d. Sharp and distinct diffraction peaks were visible in the XRD spectra, indicating that the samples were extremely crystalline. The diffraction peaks

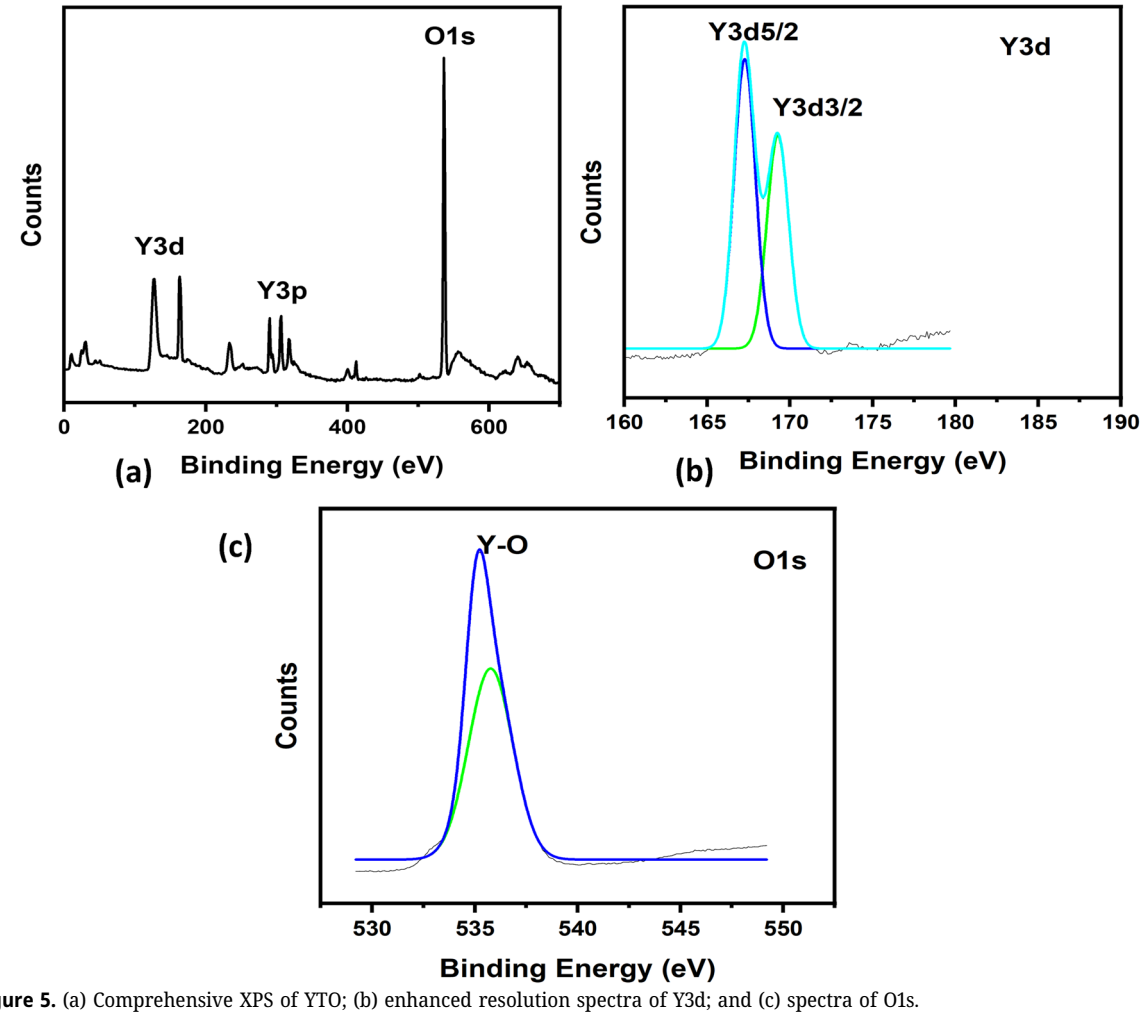

Figure 5. (a) Comprehensive XPS of YTO; (b) enhanced resolution spectra of Y3d; and (c) spectra of O1s.

were indexed to the cubic phase of YTOs. The most intense peaks appeared at characteristic 2θ values, corresponding to the (222), (400), (440), and (622) crystal planes, which are typical of cubic YTOs. Overall, the XRD results confirmed the successful synthesis of phase-pure YTO nanoparticles with high crystallinity [38].

The FTIR spectra of YTO nanoparticles, as depicted in Figure 4a, have three major absorption bands. The first band, in the range of 600–1,400 cm^{-1}, is related to the stretching vibrations of the Y–O bond, validating the existence of YTO. The second band, within the range of 1,500–2,500 cm^{-1}, is associated to the asymmetric stretching vibrations of the C–O band. This is probably due to the uptake of atmospheric CO_2, even in the absence of precursors containing C–O during the synthesis. The O–H stretching vibrations of water molecules are responsible for the third band, which is located between 3,000 and 3,500 cm^{-1}. This frequency range is ascribed to water absorption by either KBr pellets, which are used as a reference material, or by YTO nanoparticles from the ambient atmosphere [39]. With decreasing particle size, surface effects are more significant, resulting in increased adsorption characteristics. The UV–Vis absorption spectrum of the prepared YTO nanoparticles (Figure 4b) displays a sharp absorption edge around 280 nm, which can be assigned to the fundamental bandgap transition of YTOs (5.5–5.8 eV). The absorption intensity is gradually decreased with increasing wavelength with weak shoulder-like features present in the 300–400 nm range. These characteristics may be attributed to intrinsic defect states, which are mainly oxygen vacancies and surface-related energy levels, that create localized states within the bandgap and enable sub-bandgap absorption. The broad, weak band found in the range 350–380 nm could be caused by charge-transfer transitions of oxygen vacancy states. The

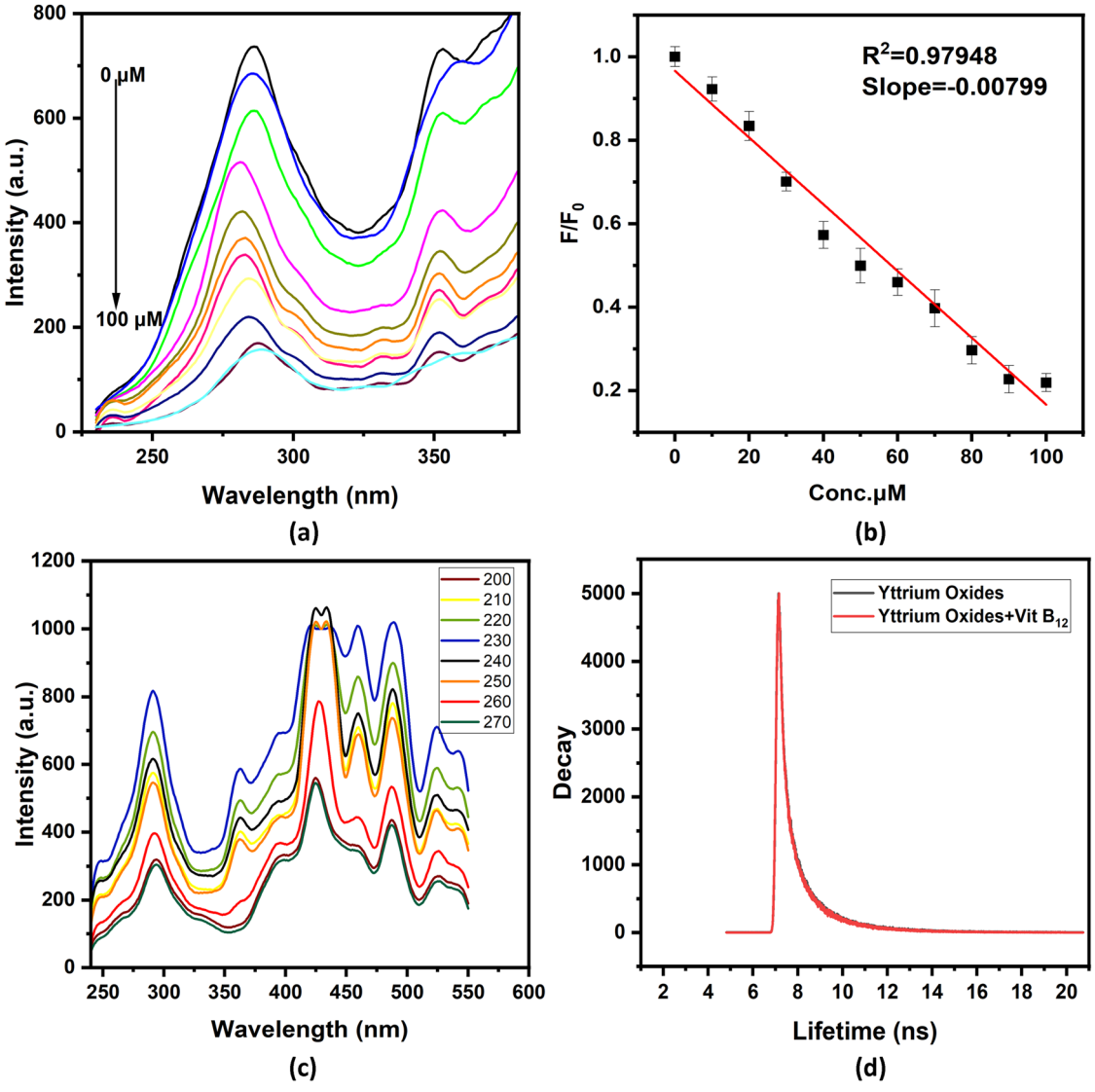

Figure 6. (a) PL spectra of YTO quenching with vitamin B_{12}, (b) linear calibration of fluorescence intensity with vitamin B_{12}, (c) excitation dependent emission spectra of YTO, and (d) fluorescence lifetime of pure YTOs nanoparticles and mixture with vitamin B_{12}.

fact that these defect-related absorptions are present confirms the nanoscale character of the material and the effect of surface chemistry on its optical behavior, which can be the key to its future applications in photocatalysis and optoelectronic devices [40–42].

Figure 5a illustrates the full-scan XPS survey spectra of YTO nanoparticles. The deconvoluted Y3d spectra in Figure 5b reveal two main peaks at 167.4 and 170.5 eV corresponding to $Y3d_{5/2}$ and $Y3d_{3/2}$, respectively. Moreover, the O1s spectrum (Figure 5c) displays a peak of deconvolution at 535.7 eV corresponding to O–Y bonding, indicating that YTO was formed successfully [43,44].

3.2 Vitamin B_{12} detection with nanosensor YTO

Researchers looked at YTO ability for usage in fluorescence sensors due to its remarkable photostability and fluorescent properties. The investigation encompassed lysine, glycine, sodium chloride, alanine, riboflavin, biotin, yttrium nitrate, dopa, phenylalanine, tryptophan, and melatonin, which include amino acids, vitamins, and metal ions. Selectivity plots illustrate the material's selectivity for vitamin B_{12}, revealing that only vitamin B_{12} significantly reduces the fluorescence spectra of YTO. The fluorescence intensity of

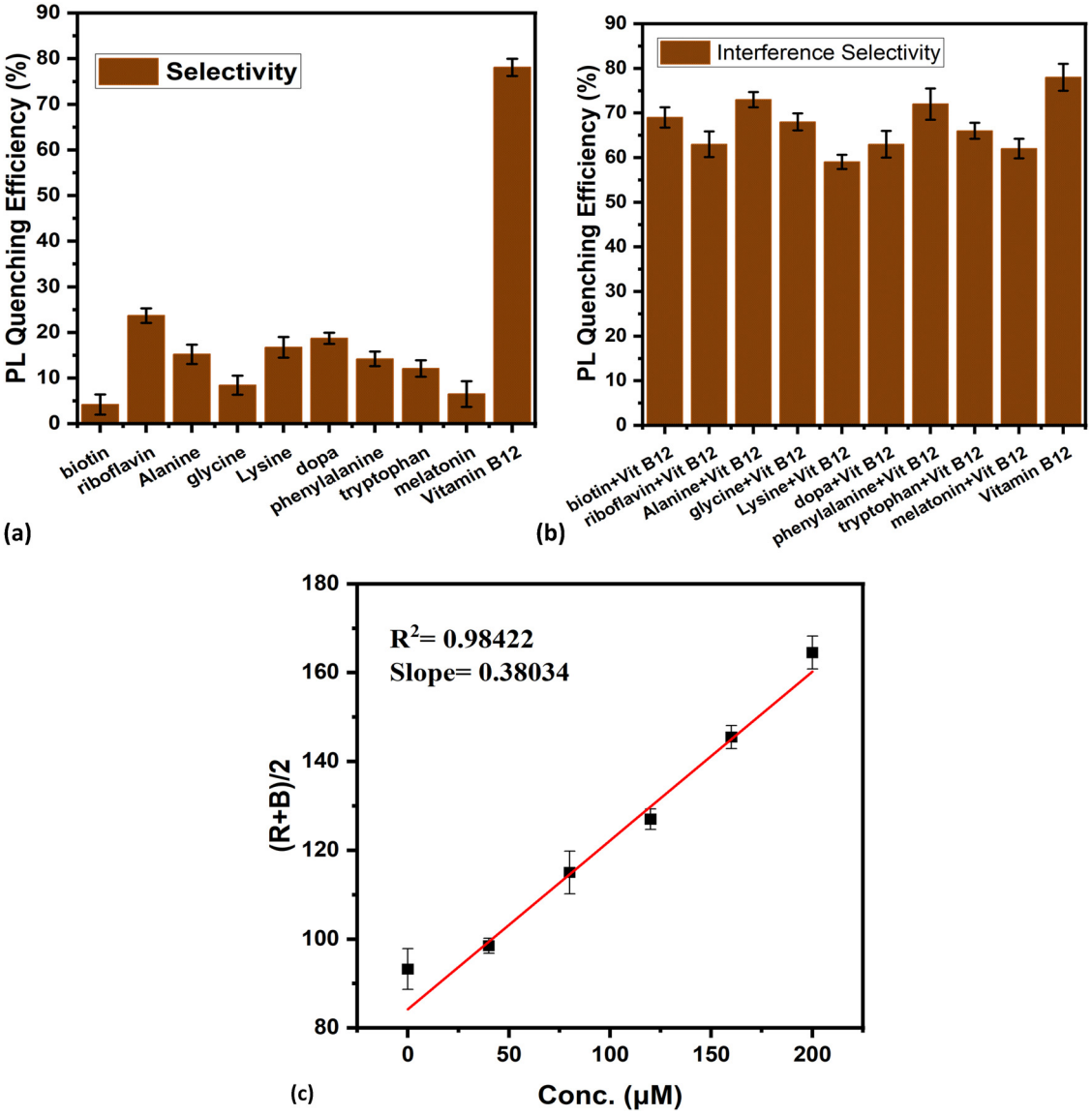

Figure 7. (a) Selectivity plot of YTO with various analytes, (b) interference selectivity plot of YTO with various analytes in the presence of vitamin B_{12}, and (c) RBG-based detection of vitamin B_{12} with YTO.

YTO at 285 nm gradually decrease as vitamin B_{12} concentrations (10–100 μM) rise, as seen in Figure 6a, demonstrating the nanosensor's ability to reliably and precisely detect vitamin B_{12}. A strong linear relationship was observed between the fluorescence ratio (F/F0) and vitamin B_{12} concentrations in the range of 10–100 μM. Figure 6b shows the titration procedure and the linear connection (R^2 = 0.97948) between YTO and vitamin B12. Moreover, it has been determined that the detection of vitamin B_{12} has a limit of detection (LOD) of 18.37 μM and a quantification limit of 55.66 μM, which is much higher than the capabilities of current methods. These results all support the excellent sensitivity and high selectivity of the "turning-off" fluorescence nanosensor for specific vitamin B_{12} identification in sample analysis. The LOD/ limit of quantification values achieved are at the micromolar level, which is above clinically significant nanomolar levels of vitamin B_{12}. This work is therefore a proof-of-concept, and future efforts will concentrate on enhancing sensitivity by nanoparticle surface modification and experimental optimization.

Sample	Spikey	Found	% Recovery	R.S.D
Urine	20	20.23	101.15	1.235
	40	40.86	102.15	1.527
	60	59.29	98.82	0.853
	80	78.45	98.06	2.245

Table 1. Vitamin B_{12} real sample studies using YTOs.

3.3 Sensing mechanism

Fluorescence quenching is a decrease in the fluorescence emission intensity of probe-detecting molecules by ground-state complex formation, energy transfer, molecular interactions, and collision processes. Typical quenching processes include photoinduced electron transfer (PET) and fluorescence resonance energy transfer (FRET) [45,46]. PET is often associated with observable changes in fluorophore lifetime [47]. In this work, FRET can be eliminated since the positively charged YTO nanoparticles render the sub 10 nm donor-acceptor distances necessary for FRET improbable under mildly basic to neutral conditions (pH 7–8). The reduction in fluorescence observed is mainly due to the inner filter effect (IFE), an optical event brought about by the overlap of the quencher's UV absorption spectrum with the fluorophore's excitation or emission spectrum. In contrast to real quenching events involving molecular interactions, IFE is independent of temperature and gives a way of distinguishing it from dynamic quenching. Fluorescence lifetime measurements on the nanoparticles before and after mixing with vitamin B_{12} further corroborated the dominance of the IFE mechanism. The addition of vitamin B_{12} did not significantly alter the fluorescence lifetime, which remained at 8.4 ns before and 8.2 ns after. This indicates that the decrease in fluorescence intensity is due to the IFE rather than FRET, as shown in Figure 6d. Moreover, quenching can be static or dynamic: static quenching is the creation of a ground-state non-emissive complex, whereas dynamic quenching occurs as a result of collisional interactions. The Stern–Volmer plot (Figure 6b) is highly linear, reflecting that the observed quenching is largely static, with IFE being the major contributor [48,49].

3.4 Selectivity

The main factor influencing YTO selectivity is the specific identification of vitamin B_{12}. The fluorescence response of YTO was compared with that of several different metal salts, vitamins, and amino acids to determine the degree of selective sensing activity. The PL intensity of several other analytes with comparable chemical structures, including glycine, alanine, lysine, sodium chloride, riboflavin, biotin, yttrium nitrate, dopa, tryptophan, phenylalanine, and melatonin, were tested to verify the selectivity of the proposed sensing probe. Figure 7a shows the histogram of the fluorescence intensity response. Figure 7b shows the interference selectivity plot of various analytes with vitamin B_{12}. The selectivity analysis revealed that the fluorescence intensity of YTO was essentially unaffected by the presence of these species (100 µM).

4. Smartphone-based sensors

Smartphone-based imaging sensors and portable devices provide better accuracy than the human eye's visual detection [50,51]. For this research, an Android-based software was developed in-house to complement YTOs solution-based nanosensor. The sample was photographed by the smartphone, and the images were processed with RGB (red, green, and blue color space) software to identify color changes. To facilitate precise image acquisition, the camera was set around 6 cm away from the sample container without flash. The incremental addition of vitamin B_{12} to the solution of YTOs brought about an easily observed, naked-eye-visible color transition from light blue to dark blue. The lower LOD was made to be 51.64 µM, in the concentration range of 0–200 µM (Figure 7c). RGB profiling was subsequently applied to assess the degree of color transitions employing the camera within a smartphone with higher precision determination of vitamin B_{12} [52,53].

5. Real sample analysis

The concentration of vitamin B_{12} in human urine samples was measured with YTOs as fluorescence probes to check the reliability and usefulness of the fluorescence detection process. Spiking of the urine samples with known concentrations of vitamin B_{12} was employed for the assay validation [54,55]. Recovery of spiked vitamin B_{12} (98.06–102.15%) with relative standard deviation (0.853–2.245%) is shown in Table 1. These findings prove that the established fluorescence method is reliable and accurate for determining vitamin B_{12} in human urine samples. Given the excellent recovery and precision observed, this method has

potential applications for other biological fluids, such as serum, which can be explored in future research.

6. Conclusion

This work successfully synthesized fluorescent YTO nanoparticle for the sensitive and selective detection of vitamin B_{12}, leveraging its interaction with YTO for precise fluorometric measurements. Comprehensive spectroscopic and microscopic characterization confirmed the structural and optical properties of the nanoparticles. The wavelengths of 230 and 285 nm were found to be the most effective for excitation and emission, respectively. Key analytical parameters, including pH, incubation time, and NaCl concentration, were systematically optimized, yielding a linear calibration range of 10–100 µM. The method demonstrated reliability, with detection and quantification limits of 18.37 and 55.66 µM, respectively. Furthermore, an innovative RGB-based sensor was developed using these nanoparticles, enabling efficient visual detection of vitamin B_{12}. The method was successfully applied to human urine samples, achieving high precision and satisfactory recoveries, underscoring its potential for real-world biomedical and analytical applications.

Acknowledgements

The authors extend their appreciation to Taif University, Saudi Arabia, for supporting this work through project number (TU-DSPP-2025-44).

Funding information

This research was funded by Taif University, Saudi Arabia, Project No. (TU-DSPP-2025-44).

Author contributions

Salma Alshehri: Writing – Review & Editing, Formal analysis; Mohammad Shariq: Supervision, Writing – Original Draft, Writing – Review & Editing; Project administration; Wafa Al-Gethami: Project administration, Writing – Review & Editing, Formal analysis; Aisha H. Al-Moubaraki: Validation, Writing – Review & Editing, software; M. D. Alshahrani: Validation; Writing – Review & Editing, resources; Nouf Alharbi: Visualization, Writing – Review & Editing, Resources; Hind S. Alzahrani: Writing – Review & Editing; Noha Al-Qasmi: Validation.

Conflict of interest statement

The authors declare no competing financial or personal interests.

Data availability statement

The data that support the findings of this study are available upon reasonable request from the authors.

References

[1] Chaudhary, P., Fatima, F., Kumar, A., Relevance of nanomaterials in food packaging and its advanced future prospects, J. Inorg. Organomet. Polym. Mater., 2020, 30: 5180–5192

[2] Aresta, A., Calvano, C.D., Trapani, A., Cellamare, S., Zambonin, C.G., De Giglio, E., Development and analytical characterization of vitamin(s)-loaded chitosan nanoparticles for potential food packaging applications, J. Nanopart. Res., 2013, 15: 1592

[3] Jafari, M, Mousavi, M., Shirzad, K., Hosseini, M.A., Badiei, A., Pourhakkak, P., et al., A TiO_2 nanotube array decorated by Ag nanoparticles for highly sensitive SERS determination and self-cleaning of vitamin B12, Microchem. J., 2022, 181: 107813

[4] Schmidt, A., Call, L.M., Macheiner, L., Mayer, H.K., Determination of vitamin B12 in four edible insect species by immunoaffinity and ultra-high performance liquid chromatography, Food Chem., 2019, 281: 124–129

[5] Layden, A.J., Täse, K., Finkelstein, J.L., Neglected tropical diseases and vitamin B12: a review of the current evidence, Trans. R. Soc. Trop. Med. Hyg., 2018, 112: 423–435

[6] Duhan, J., Saini, S., Kumar, H., Obrai, S., BPGQD/g-C_3N_4 nanocomposites as sensitive and selective platform for fluorescence and RGB based detection of vitamin B_{12}, J. Lumin., 2024, 275: 120764

[7] Zhu, X., Wang, X., Zhang, C., Wang, X., Gu, Q., A riboswitch sensor to determine vitamin B12 in fermented foods, Food Chem., 2015, 175: 523–528

[8] Antherjanam, S., Saraswathyamma, B., Krishnan, R.G., Gopakumar, G.M., Electrochemical sensors as a versatile tool for the quantitative analysis of vitamin B12, Chem. Pap., 2021, 75: 2981–2995

[9] Gharibzahedi, S.M.T., Moghadam, M., Amft, J., Tolun, A., Hasabnis, G., Altintas, Z., Recent advances

in dietary sources, health benefits, emerging encapsulation methods, food fortification, and new sensor-based monitoring of vitamin B12: a critical review, Molecules, 2023, 28: 7469

[10] Lu, Q., Feng, Y., Zhou, Q., Yang, T., Kuang, H., Xu, C., et al., A time-resolved fluorescent microsphere immunochromatographic assay for determination of vitamin B12 in infant formula milk powder, Biosensors, 2025, 15: 65

[11] Jardan, Y.A.B., Mostafa, A.M., Barker, J., Ali, A.B.H., El-Wekil, M.M., A novel route for fabrication of yellow emissive carbon dots for selective and sensitive detection of vitamin B12, Anal. Methods, 2025, 17: 3007–3016

[12] Gharibzahedi, S.M.T., Hasabnis, G.K., Akin, E., Altintas, Z., Molecularly imprinted polymers-based electrochemical sensors for tracking vitamin B12 released from spray-dried microcapsules during in vitro simulated gastrointestinal digestion, Sens. Bio-Sens. Res., 2025, 47: 100759

[13] Almutib, E., Alasmari, A., Alhashmialameer, D., Algarni, Z.S., Alrahili, M.R., Alzahrani, A., et al., Characterization of cobalt-substituted cadmium ferrites $CoxCd_{1-x}Fe_2O_4$: structural, optical, and magnetic insights, Appl. Phys. A, 2025, 131: 77

[14] Shariq, M., Madkhli, A.Y., Kawtherali, S.F., Alshehri, K., Alasmari, A., Algarni, Z.S., et al., Recent advancement in development of nitrogen-doped CQDs for dye sensitized solar cell and photodetector: a review, Surf. Interfaces, 2025, 59: 10591

[15] Hussain, M., Hussaini, S.S., Shariq, M., Althikrallah, H.A., Al-Qasmi, N., Seku, K., et al., Efficient removal of rhodamine B dye using myrrh-based magnetized multi-walled carbon nanotubes as adsorbent, Adsorption, 2024, 30: 1925–1936

[16] Alhashmialameer, D., Shariq, M., Althikrallah, H.A., Al-Amari, M., BaQais, A., Alayyafi, A.A., et al., Hydrothermally synthesized Nb-doped TiO_2 nanosheets for efficient removal of methylene blue dye on photocatalytic performance, Phys. Scr., 2024, 99: 085915

[17] Qamar, M.A., Al-Gethami, W., Alaghaz, A.N.M.A., Shariq, M., Mohammed, A., Areshi, A.A., et al., Progress in the development of phyto-based materials for adsorption of dyes from wastewater: a review, Mater. Today Commun., 2024, 38: 108385

[18] Hussain, M, Hussaini, S.S., Shariq, M., Alzahrani, H., Alholaisi, A.A., Alharbi, S.H., et al., Enhancing Cu^{2+} ion removal: an innovative approach utilizing modified frankincense gum combined with multiwalled carbon tubes and iron oxide nanoparticles as adsorbent, Molecules, 2023, 28: 4494

[19] Magdalane, C.M., Kaviyarasu, K., Vijaya, J.J., Siddhardha, B., Jeyaraj, B., Facile synthesis of heterostructured cerium oxide/yttrium oxide nanocomposite in UV light induced photocatalytic degradation and catalytic reduction: synergistic effect of antimicrobial studies, J. Photochem. Photobiol. B Biol., 2017, 173: 23–34

[20] El-Shafai, N.M., Ramadan, M.S., El-Mehasseb, I.M., Decoration of modified self-assembly membrane by magnesium oxide and yttrium oxide nanoparticles for biosensors, supercapacitors, and water treatment, Int. J. Energy Res., 2022, 46: 18029–18048

[21] Rajakumar, G., Mao, L., Bao, T., Wen, W., Wang, S., Gomathi, T., et al., Yttrium oxide nanoparticle synthesis: an overview of methods of preparation and biomedical applications, Appl. Sci., 2021, 11: 2172

[22] Sun, H., Yao, B., Han, Y., Yang, L., Zhao, Y., Wang, S., et al., Multi-interface engineering of self-supported nickel/yttrium oxide electrode enables kinetically accelerated and ultra-stable alkaline hydrogen evolution at industrial-level current density, Adv. Energy Mater., 2024, 14: 2303563

[23] Yousaf, F., Irfan, M., Plant-mediated synthesis of yttrium oxide nanoparticles vs. traditional methods: current trends and potential applications, BioNanoScience, 2024, 14: 3889–3905

[24] Niederberger, M., Pinna, N., Metal oxide nanoparticles in organic solvents: synthesis, formation, assembly and application, Springer Sci. Bus. Media, 2009

[25] Curtis, C.E., Properties of yttrium oxide ceramics, J. Am. Ceram. Soc., 1957, 40: 274–278

[26] Sowjanya, M., Shariq, M., Alajlani, Y., Pamu, D., Chowdhruy, R., Jayaganthan, R., et al., Effect of Ar: O_2 gas atmosphere on optical properties of Y_2O_3-doped ZnO thin films by RF sputtering, Europhys. Lett., 2022, 129(3), 34003

[27] Wang, Y.-Y., Gao, M.-Y., Liu, S., Li, G.-R., Gao, X.-P., Yttrium surface gradient doping for enhancing structure and thermal stability of high-Ni layered oxide as cathode for Li-ion batteries, ACS Appl. Mater. Interfaces, 2021, 13: 7343–7354

[28] Govindasamy, R., Govindarasu, M., Alharthi, S.S., Mani, P., Bernaurdshaw, N., Gomathi, T., et al., Sustainable green synthesis of yttrium oxide (Y_2O_3) nanoparticles using *Lantana camara* leaf extracts: physicochemical characterization, photocatalytic degradation, antibacterial, and anticancer potency, Nanomaterials, 2022, 12: 2393

[29] Jay Chithra, M., Sathya, M., Pushpanathan, K.J.A.M.S., Effect of pH on crystal size and photoluminescence

property of ZnO nanoparticles prepared by chemical precipitation method, Acta Metall. Sin. (Eng. Lett.), 2015, 28: 394–404

[30] Chen, C., He, H., Lu, Y., Wu, K., Ye, Z., Surface passivation effect on the photoluminescence of ZnO nanorods, ACS Appl. Mater. Interfaces, 2013, 5: 6354–6359

[31] Duhan, J., Obrai, S., Highly sensitive and selective fluorescence and smartphone-based sensor for detection of L-dopa using nitrogen sulphur graphene quantum dots, Microchem. J., 2023, 193: 109262

[32] Den Engelsen, D., Harris, P.G., Ireland, T.G., Fern, G., Silver, J., Symmetry-related transitions in the spectrum of nanosized cubic Y_2O_3:Tb^{3+}, ECS J. Solid. State Sci. Technol., 2015, 4: R105–R113

[33] Kohlmann, T., Goez, M., Combined static and dynamic intramicellar fluorescence quenching: effects on stationary and time-resolved Stern–Volmer experiments, Phys. Chem. Chem. Phys., 2019, 21: 10075–10085

[34] Duhan, J., Obrai, S., Samarium, nitrogen co-doped carbon dots for detection of epinephrine: theoretical and experimental, J. Ind. Eng. Chem., 2025, 142: 582–592

[35] Chapman, J., Truong, V.K., Elbourne, A., Gangadoo, S., Cheeseman, S., Rajapaksha, P., et al., Combining chemometrics and sensors: toward new applications in monitoring and environmental analysis, Chem. Rev., 2020, 120: 6048–6069

[36] Kumar, P.S., Sundaramurthy, J., Sundarrajan, S., Babu, V.J., Singh, G., Allakhverdiev, S.I., et al., Hierarchical electrospun nanofibers for energy harvesting, production and environmental remediation, Energy Environ. Sci., 2014, 7: 3192–3222

[37] Gai, S., Li, C., Yang, P., Lin, J., Recent progress in rare earth micro/nanocrystals: soft chemical synthesis, luminescent properties, and biomedical applications, Chem. Rev., 2014, 114: 2343–2389

[38] Duhan, J., Obrai, S., Lanthanum nitrogen co-doped carbon quantum dots as optical and smartphone sensors for serotonin detection, Opt. Mater., 2023, 145: 114466

[39] Srinivasan, R., Yogamalar, R., Bose, A.C., Structural and optical studies of yttrium oxide nanoparticles synthesized by co-precipitation method, Mater. Res. Bull., 2010, 45: 1165–1170

[40] Viswanath, R., Naik, H.S.B., Somalanaik, Y.K.G., Neelanjeneallu, P.K.P., Harish, K.N., Prabhakara, M.C., Studies on characterization, optical absorption, and photoluminescence of yttrium doped ZnS nanoparticles, J. Nanotechnol., 2014, 2014: 924797–924798

[41] Parangusan, K., Subramanium, V., Sundarabharathi, L., Kannan, K., Radhika, D., Influence of pH on structural, morphological, optical, photocatalytic, and antibacterial properties of yttrium oxide nanoparticles via co-precipitation method, Mater. Chem. Phys., 2021, 276: 125431

[42] Hu, J., Sun, Y., Aryee, A.A., Qu, L., Zhang, K., Li, Z., Mechanisms for carbon dots-based chemosensing, biosensing, and bioimaging: a review, Anal. Chim. Acta, 2022, 1209: 338885

[43] Tanwar, A.S., Hussain, S., Malik, A.H., Afroz, M.A., Iyer, P.K., Inner filter effect based selective detection of nitroexplosive-picric acid in aqueous solution and solid support using conjugated polymer, ACS Sens., 2016, 1: 1070–1077

[44] Oladipo, A.A., Oskouei, S.D., Gazi, M., Metal-organic framework-based nanomaterials as opto-electrochemical sensors for the detection of antibiotics and hormones: a review, Beilstein J. Nanotechnol., 2023, 14: 631–673

[45] Singh, D.P., Inamdar, S.R., Kumar, S., Fluorescence spectrometry, in Modern Techniques of Spectroscopy: Basics, Instrumentation, and Applications, 2021, pp. 431–468

[46] Duhan, J., Obrai, S., Sodium vanadates doped boron phosphorus graphene quantum dots: a novel nanosensor for the fluorescence detection of rutin, Food Chem., 2024, 460: 140630

[47] Kannouma, R.E., Kamal, A.H., Hammad, M.A., Mansour, F.R., Tips and tricks for applying luminescent carbon dots in chemical analysis: recent advancements, obstacles, and future outlook, Microchem. J., 2024, 192: 111667

[48] Ahmad, M., Bushra, R., Ritzoulis, C., Pectin–mucin interactions: insights from fluorimetry, thermodynamics and dual (static and dynamic) quenching mechanisms, Int. J. Biol. Macromol., 2024, 277: 134564

[49] Hunt, B., Ruiz, A.J., Pogue, B.W., Smartphone-based imaging systems for medical applications: a critical review, J. Biomed. Opt., 2021, 26: 040902

[50] Banik, S., Melanthota, S.K., Arbaaz, Vaz, J.M., Kadambalithaya, V.M., Hussain, I., et al., Recent trends in smartphone-based detection for biomedical applications: a review, Anal. Bioanal. Chem., 2021, 413: 2389–2406

[51] Duhan, J., Kumar, H., Obrai, S., Fabrication and DFT study of IFE based nano-sensor for fluorometric detection of norepinephrine, Opt. Laser Technol., 2024, 174: 110665

[52] Kumar, H., Duhan, J., Obrai, S., Highly sensitive and selective fluorescence and smartphone-based

sensor for detection of rutin using boron nitrogen co-doped graphene quantum dots, J. Fluoresc., 2024, 34: 1–13

[53] Mohamed, G.G., Fekry, A.M., Abou Attia, F.M., Ibrahim, N.S., Azab, S.M., Simultaneous determination of some antidepressant drugs and vitamin B12 in pharmaceutical products and urine sample using HPLC method, J. Chromatogr. B, 2020, 1150: 122178

[54] Chalissery, P., Homann, C., Stepp, H., Eisel, M., Aumiller, M., Rühm, A., et al., Influence of vitamins and food on the fluorescence spectrum of human urine, Lasers Surg. Med., 2024, 56: 485–495

[55] Noreldeen, H.A.A., Huang, K.Y., Wu, G.W., Peng, H.P., Deng, H.H., Chen, W., Deep learning-based sensor array: 3D fluorescence spectra of gold nanoclusters for qualitative and quantitative analysis of vitamin B6 derivatives, Anal. Chem., 2022, 94: 9287–9296